SCIENTIFIC REPORTS

OPEN

Hybrid Nanostructured Porous Silicon-Silver Layers for Wideband Optical Absorption

Received: 18 December 2018
Accepted: 23 April 2019
Published online: 13 May 2019

Raúl J. Martín-Palma[1,2], Patrick D. McAtee[3], Rehab Ramadan[2,4] & Akhlesh Lakhtakia[3]

As subwavelength nanostructures are receiving increasing attention for photonic and plasmonic applications, we grew nanostructured porous silicon (n-PS) and hybrid n-PS/Ag layers onto silicon substrates and measured their reflection and absorption characteristics as functions of the wavelength, angle of incidence, and polarization state of incident light. The experimental results show that the absorption characteristics of the hybrid n-PS/Ag layer can be controlled by selecting the appropriate combination of its thickness and porosity, together with the density of infiltrant silver nanoparticles. The observed wideband optical absorption characteristics of the hybrid n-PS/Ag layers might be useful in light-harvesting devices and photodetectors, since the overall efficiency will be increased as a result of increased field-of-view for both *s*- and *p*-polarization states of incident light.

Although nanostructured porous silicon (n-PS) was discovered by Uhlir in 1956 while studying electropolishing of silicon and germanium in HF-based solutions[1], it was not until the observation visible photoluminescence from room-temperature n-PS by Canham in 1990[2] that this material was envisaged as a good candidate for applications in the field of photonics. Since then, its many additional properties beyond photo- and electro-luminescence have resulted in several successful applications in different fields ranging from microelectronics to biomedicine[3].

Nanostructured porous silicon can be described quite simply as an amorphous matrix in which silicon nanocrystals are embedded[4–7]. The morphology of a n-PS sample depends on strongly on the specific fabrication parameters, including electrolyte composition and fabrication current density[8]. The complex-valued effective refractive index of n-PS is therefore dependent on the electrochemical fabrication parameters[9]. Control over the refractive index allows the use of n-PS for tunable photonic structures made entirely of silicon[10]. It is worth pointing out that the electrochemical technique used for the fabrication of n-PS is compatible with current CMOS fabrication processes, thus enabling the potential integration of n-PS into circuits using microelectronics-compatible procedures.

Within this context and given the increasing attention being received by subwavelength nanostructures for photonic and plasmonic applications[11,12], we decided to explore the use of n-PS and hybrid n-PS/Ag layers grown onto silicon as wideband optical absorbers. Therefore, we experimentally investigated the dependence of optical absorption characteristics of n-PS and hybrid n-PS/Ag layers on the thickness and porosity of n-PS layers and the amount of silver infiltrating the pores of n-PS. More specifically, we measured the reflection and absorption characteristics of the n-PS and hybrid n-PS/Ag layers as functions of the wavelength, angle of incidence, and polarization state of incident light.

Experimental

Fabrication of n-PS and hybrid n-PS/Ag layers. Nanostructured porous silicon layers were formed by the electrochemical etching of boron-doped (*p*-type) silicon wafers of <100> orientation, resistivity in the 0.01–0.02 Ω·cm range, and surface roughness on the order of 0.1 nm. The wafers were cut into $1.5 \times 1.5\,cm^2$ pieces. Each piece was mounted in a sample holder with about $1.23\,cm^2$ area exposed to the etching solution, which was formulated as a 1:2 HF (48 wt %):ethanol (98 wt %) mixture. The anodization times, ranging from 18–46 s, were adjusted to obtain layers of three different thickness. Two different current densities — namely, 20 and $60\,mA/cm^2$ — were used, leading to two different porosities arising from the creation of nanocolumnar pores

[1]Department of Materials Science and Engineering, The Pennsylvania State University, University Park, Pennsylvania, PA, 16802, USA. [2]Departamento de Física Aplicada, Universidad Autónoma de Madrid, 28049 Cantoblanco, Madrid, Spain. [3]Department of Engineering Science and Mechanics, The Pennsylvania State University, University Park, Pennsylvania, PA, 16802, USA. [4]Department of Physics, Faculty of Science, Minia University, 61519, Minia, Egypt. Correspondence and requests for materials should be addressed to R.J.M.-P. (email: raul@psu.edu)

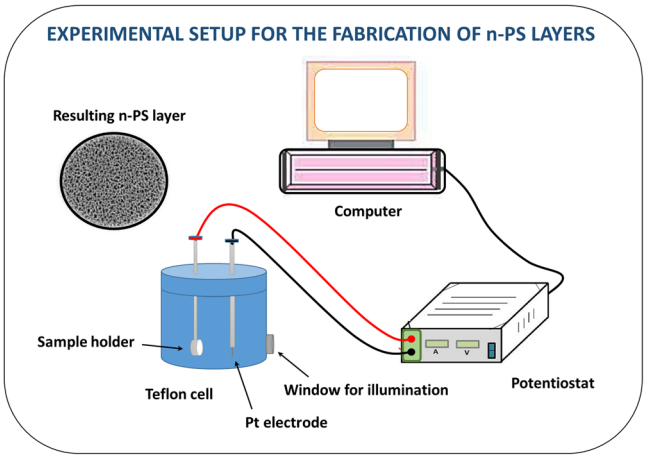

Figure 1. Experimental setup used for the fabrication of n-PS layers by the electrochemical etch of silicon wafers.

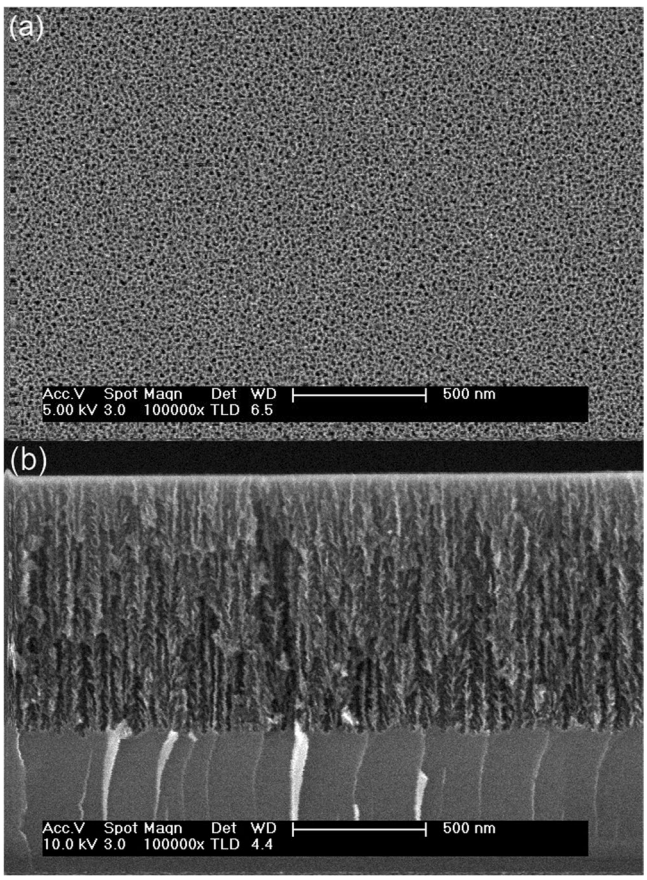

Figure 2. (**a**) Top-view and (**b**) cross-sectional FESEM images of a typical high-porosity n-PS layer (fabrication current density of 60 mA/cm^2).

of two different average diameters. After fabrication, each sample was rinsed in ethanol and blown dry with a mild stream of dry nitrogen. The experimental setup used for the fabrication of n-PS layers by the electrochemical etch of silicon wafers is schematically depicted in Fig. 1.

The n-PS layer was used as a template for the subsequent growth of silver nanoparticles inside the porous structure. For this task, a modified electrochemical deposition process[13] was implemented. This process was carried out using a Bio-Logic SP-150 potentiostat at a fixed current density of 1 μA/cm^2 for different electrodeposition durations (2, 4, 6 or 15 min) in an aqueous solution of silver nitrate (0.1 mM), sodium citrate (0.25 mM), and nitric acid (0.01 M), with pH = 3. Afterwards, the sample was rinsed in ethanol for 5 min and subsequently

Current density (mA/cm^2)	Duration of anodization (s)	Thickness (μm)	Duration of electrodeposition (min)
n-PS and hybrid n-PS/Ag layers			
20 (low porosity)	22	0.33	0
	33	0.60	0
	46	0.77	0
60 (high porosity)	18	0.70	0
	28	1.00	0
	40	1.40	0
60 (high porosity)	18	0.70	2, 4, 6, or 15
	28	1.00	2, 4, 6, or 15
	40	1.40	2, 4, 6, or 15

Table 1. Summary of the fabrication conditions of the n-PS layers and hybrid n-PS/Ag layers.

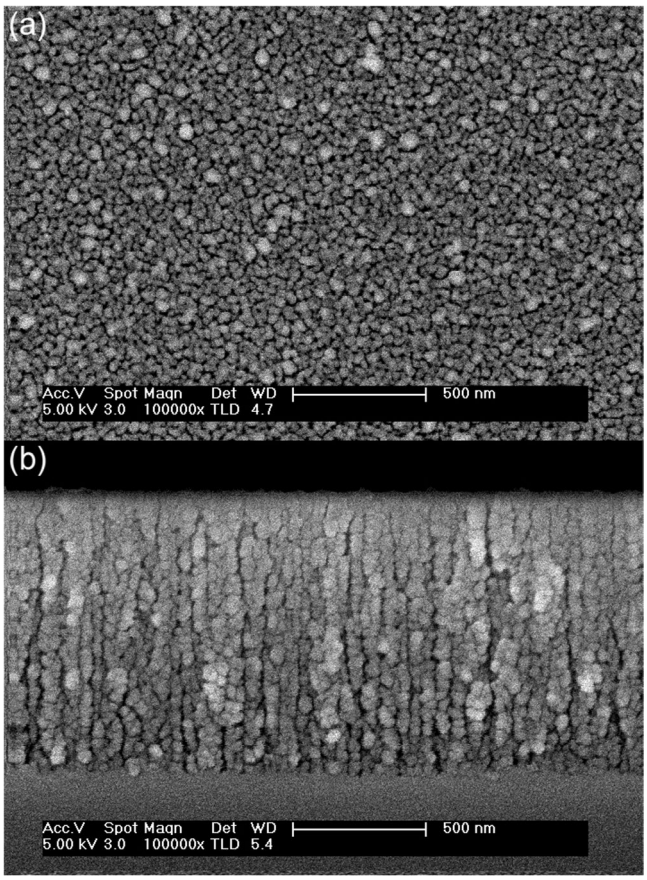

Figure 3. Top-view and cross-sectional FESEM images of a typical hybrid n-PS/Ag layer. The n-PS layer was grown using a current density of 60 mA/cm^2 and the silver nanoparticles were electrodeposited for 4 min. The Ag nanoparticles (bright areas) are rounded with diameters in the 30–65 nm range.

distilled in water for another 5 min and finally dried with a mild stream of dry nitrogen. This process leads to the formation of a hybrid n-PS/Ag thin film.

In all, four different sets of n-PS and hybrid n-PS/Ag layers were prepared as detailed in Table 1, to study the effects of porosity, thickness, and the volumetric proportion of silver on the optical response characteristics.

Morphological characterization. Top-view and cross-sectional images of every sample were acquired using a Philips XL 30S-FEG field emission scanning electron microscope (FESEM). The sizes of the pores of n-PS and the Ag nanoparticles were determined from these FESEM images using the ImageJ software.

Optical characterization. *Specular reflection.* White light from a halogen source (HL-2000, Ocean Optics, Dunedin, Florida, USA) was passed through a fiber-optic cable and then through a linear polarizer

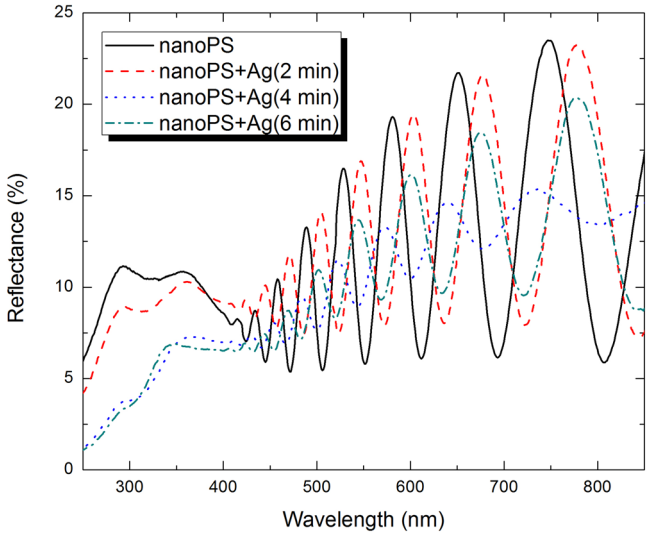

Figure 4. Overall reflectance spectra of 1.4-μm-thick high-porosity n-PS and hybrid n-PS/Ag layers for different durations of infiltration of silver nanoparticles by electrodeposition (2, 4, and 6 min).

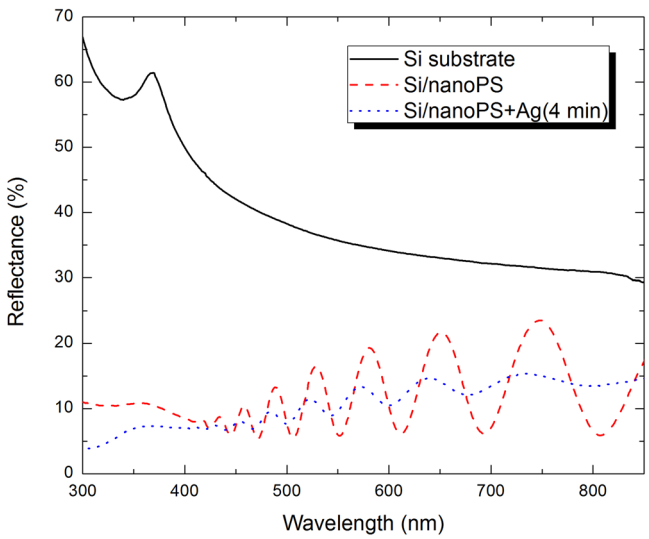

Figure 5. Overall reflectance spectra of bulk silicon substrate, a 1.4-μm-thick high-porosity n-PS layer on a silicon substrate, and a 1.4-μm-thick high-porosity n-PS layer (on a silicon susbtrate) infiltrated by silver nanoparticles during 4-min electrodeposition.

(GT10, ThorLabs, Newton, NJ, USA) to be incident upon the sample to be characterized. The reflected light was passed through a second linear polarizer (GT10, ThorLabs) and then through a fiber-optic cable to a CCD spectrometer (HRS-BD1-025, Mightex Systems, Pleasanton, CA, USA). All measurements were taken in a dark room and background noise was removed from the measured data. Co-polarized specular reflectances (R_{ss} and R_{pp}) and cross-polarized specular reflectances (R_{ps} and R_{sp}) were measured for the angle of incidence θ_{inc} in the 10°−70° range as functions of the free-space wavelength λ_o in the 400–900 nm visible and near-infrared spectral regimes. The angle of incidence is measured with respect to the perpendicular to the illuminated face of the sample, with $\theta_{inc} = 0°$ for normal incidence. The first subscript on a specular reflectance denotes the linear polarization state of light collected by the detector, while the second subscript denotes the linear polarization state of light impinging on the sample. Care was taken to remove the effects of ambient light, as described elsewhere[14].

Overall reflection. The overall reflectance spectrum for λ_o in the 250–900 nm wavelength regime was acquired using a double-beam spectrophotometer (V-560, JASCO International, Tokyo, Japan) equipped with an integrating sphere in order to collect both diffuse and specular reflections, with unpolarized light being incident at angle $\theta_{inc} = 10°$ (i.e., almost normally) on the sample. The photometric accuracy is specified by the manufacturer to be better than 0.3%.

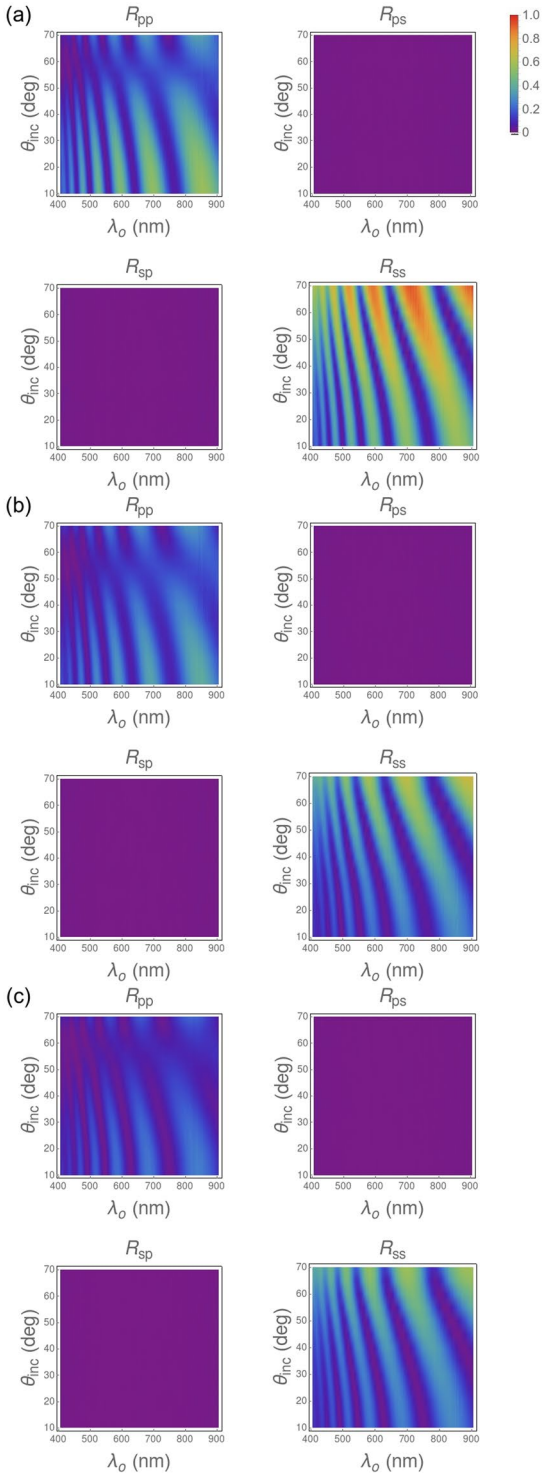

Figure 6. Dependences on λ_o and θ_{inc} of the measured specular reflectances of (**a**) a 1-μm-thick high-porosity n-PS layer, (**b**) a 1-μm-thick high-porosity hybrid n-PS/Ag layer after silver infiltration for 15 min, and (**c**) a 1-μm-thick high-porosity hybrid n-PS/Ag layer after silver infiltration for 4 min.

Experimental Results

Figure 2 shows top-view and cross-sectional FESEM images of a typical n-PS layer grown by the electrochemical etch of a monocrystalline silicon wafer. Clearly, the electrochemical fabrication process delivers a porous columnar structure. For low-porosity n-PS layers (fabrication current density of 20 mA/cm^2), the pore diameter is in the 5–15 nm range, as determined from FESEM image analysis, but that range changes to 15–35 nm in the case of high-porosity n-PS layers (60 mA/cm^2).

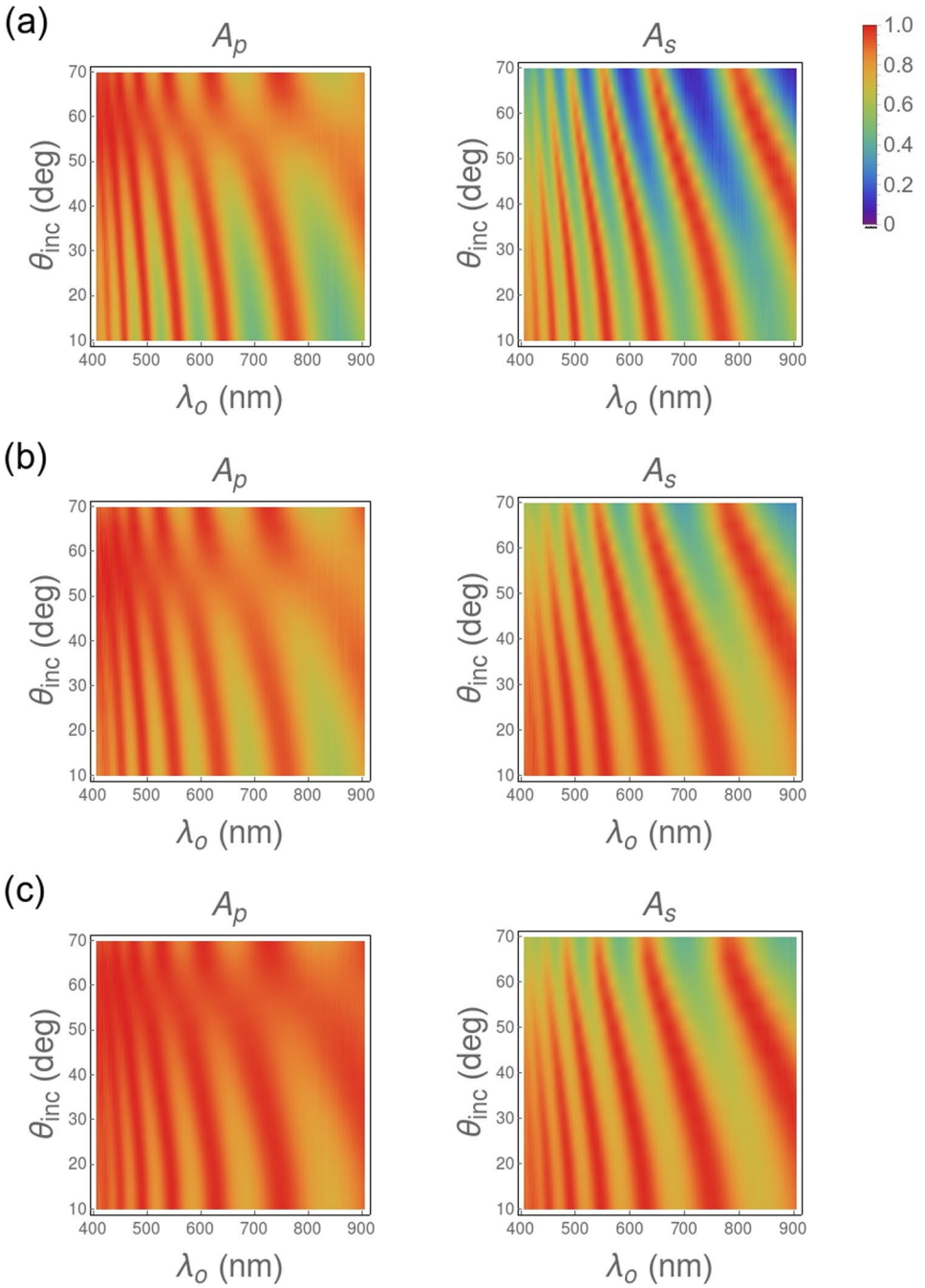

Figure 7. Dependences on λ_o and θ_{inc} of the absorptances of (**a**) a 1-μm-thick high-porosity n-PS layer, (**b**) a 1-μm-thick high-porosity hybrid n-PS/Ag layer after silver infiltration for 15 min, and (**c**) a 1-μm-thick high-porosity hybrid n-PS/Ag layer after silver infiltration for 4 min.

In Fig. 3, top-view and cross-sectional FESEM images of a typical hybrid n-PS/Ag layer grown onto silicon are presented. The sample comprises a high-porosity n-PS layer (current density 60 mA/cm^2) in which silver nanoparticles were infiltrated for 4 min. The FESEM images show that the fabrication process leads to a quite homogeneous distribution of silver nanoparticles on the surface and inside the n-PS layer, the nanoparticle diameter ranging from 30–65 nm as determined by image analysis. Accordingly, given their characteristic small feature sizes, both the n-PS and the hybrid n-PS/Ag layers can be treated as homogeneous media from an optical standpoint at any wavelength λ_o exceeding about 200 nm.

Aiming at increasing optical absorption in the hybrid n-PS/Ag layers, we controlled the volumetric fraction of silver nanoparticles by using three different electrodeposition durations: namely, 2, 4, and 6 min. From the overall reflectance spectra shown in Fig. 4, we concluded that the differences between neighboring maxima and minima are the least when the electrodeposition duration was 4 min.

Reflection reduction after electrodeposition for 2 min can be attributed to increased absorption due to a strong interaction between free electrons in the silver nanoparticles and the incident electromagnetic radiation[15]. Reflection reduction is enhanced after electrodeposition for 4 min, as a consequence of increased absorption due to a larger number density of silver nanoparticles. However, increasing the electrodeposition duration to 6 min results in increased reflection, because the even larger number density of silver nanoparticles leads to the percolation effect[16,17], the hybrid n-PS/Ag layer acquiring a strongly metallic character that inhibits refraction into the layer.

The overall reflectance spectra of the high-porosity n-PS layers and the best hybrid n-PS/Ag layers are shown in Fig. 5 in addition to the overall reflectance spectrum of a silicon wafer. It is evident that the fabrication of n-PS onto silicon substrates results in a remarkable reduction of the average overall reflectance and that further reflection reduction occurs on infiltration by silver nanoparticles. This effect is attributable to increased optical absorption provided by the silver nanoparticles in consequence of the high values of the imaginary part of the refractive index of silver in the chosen spectral regime[18–20]. Additionally, the observed shifts in the reflectance maxima and minima can be attributed to the changes in the spectrum of the complex-valued effective refractive index as a consequence of: first, due to the creation of pores due to electrochemical etching and, second, to the electrodeposition of silver nanoparticles.

Figure 6 shows characteristic two-dimensional density plots of co-polarized and cross-polarized specular reflectances as functions of λ_o and θ_{inc} for a n-PS layer and two hybrid n-PS/Ag layers grown onto monocrystalline substrates. First, it is worth noticing that the two cross-polarized reflectances (R_{ps} and R_{sp}) are negligible for all n-PS layers and hybrid n-PS/Ag layers, independently of their porosity and thickness. Therefore, materials of both types can be considered to be isotropic in the plane normal to the thickness direction. Second, we found that the reflectance spectra did not change when the sample was translated transversely to the path of the incident light beam. Therefore, materials of both types can be considered to be effectively homogeneous, as also indicated by the FESEM images.

The reflectance spectra in Fig. 6 contain several bands having their origin in classical interference effects. The bright bands (or fringes) correspond to interference maxima while the dark bands correspond to interference minima. We ascertained from the reflectance spectra of all 18 samples mentioned in Table 1 that the number of bright bands increases with the sample thickness. Also, there is an evident dependence of the width of the bright bands on the angle of incidence, which is a consequence of increased optical path for larger angles of incidence.

In the plots of R_{pp} in Fig. 6, we see a dark horizontal region corresponding to low reflection in the vicinity of $\theta_{inc} = 60°$, but a similar dark region is absent in the plots of R_{ss}. This is indicative of the pseudo-Brewster effect[21]. As θ_{inc} increases further, both R_{pp} and R_{ss} increase rapidly towards unity.

We ascertained experimentally that no light was transmitted through any of the samples. Therefore, we defined the absorptances $A_p = 1 - (R_{pp} + R_{sp})$ and $A_s = 1 - (R_{ss} + R_{ps})$ and plotted them as functions of λ_o and θ_{inc} in Fig. 7 for a n-PS layer and two hybrid n-PS/Ag layers grown onto silicon substrates. Clearly in this figure, A_p is larger than A_s for all three samples. Besides, the comparison of Fig. 7a,b allows the conclusion that infiltration of n-PS layers by silver nanoparticles results in increased absorption, given that broader and more intense absorption bands are displayed. This enhancement is observed for both A_p and A_s, although it is more pronounced for A_s. Absorption is further increased once the density of silver particles in the nanoporous structure is optimized, as shown in Fig. 7c. Accordingly, it can be concluded that the infiltration of n-PS by silver nanoparticles results in increased absorption and, additionally, optical absorption can be controlled by controlling the density of the infiltrant silver nanoparticles.

Concluding Remarks

The use of nanostructured porous silicon (n-PS) and hybrid n-PS/Ag layers grown onto silicon as wideband optical absorbers with potential applications in the fields of light sensing and light harvesting was experimentally explored by investigating the dependences of the optical reflectances and absorptances on the thickness and porosity of n-PS and hybrid n-PS/Ag layers and the number density of the infiltrant silver nanoparticles.

Our data show that the absorption characteristics of the hybrid n-PS/Ag layers can be controlled by selecting the appropriate combination of thickness and porosity of the n-PS layers, together with the density of infiltrant silver nanoparticles. The wideband optical absorption characteristics of the hybrid n-PS/Ag layers are expected to contribute to increased efficiency of light-harvesting devices and photodetectors given by increased field-of-view for both *s*- and *p*-polarization states of incident light over a broad spectral regime.

References

1. Uhlir, A. Electrolytic Shaping of Germanium and Silicon. *Bell Syst. Tech. J.* **35**, 333–347 (1956).
2. Canham, L. T. Silicon quantum wire array fabrication by electrochemical and chemical dissolution of wafers. *Appl. Phys. Lett.* **57**, 1046–1048 (1990).
3. Canham, L. T. (ed.) *Handbook of Porous Silicon*, 2nd ed. (Springer 2018).
4. Martín-Palma, R. J., Pascual, L., Herrero, P. & Martínez-Duart, J. M. Direct determination of grain sizes, lattice parameters, and mismatch of porous silicon. *Appl. Phys. Lett.* **81**, 25–27 (2002).
5. Martín-Palma, R. J., Pascual, L., Landa, A., Herrero, P. & Martínez-Duart, J. M. High-resolution transmission electron microscopic analysis of porous silicon/silicon interface. *Appl. Phys. Lett.* **85**, 2517–2519 (2004).
6. Martín-Palma, R. J., Pascual, L., Herrero, P. & Martínez-Duart, J. M. Monte Carlo determination of crystallite size of porous silicon from x-ray line broadening. *Appl. Phys. Lett.* **87**, 211906–1-3 (2005).
7. Pascual, L., Martín-Palma, R. J., Landa-Cánovas, A. R., Herrero, P. & Martínez-Duart, J. M. Lattice distortion in nanostructured porous silicon. *Appl. Phys. Lett.* **87**, 251921–1-3 (2005).
8. Sailor, M. J. *Porous Silicon in Practice: Preparation, Characterization and Applications* (Wiley, 2012).
9. Torres-Costa, V., Martín-Palma, R. J. & Martínez-Duart, J. M. Optical constants of porous silicon films and multilayers determined by genetic algorithms. *J. Appl. Phys.* **96**, 4197–4203 (2004).

10. Torres-Costa, V. & Martín-Palma, R. J. Application of nanostructured porous silicon in the field of optics. A review. *J. Mater. Sci.* **45**, 2823–2838 (2010).
11. Atwater, H. A. & Polman, A. Plasmonics for improved photovoltaic devices. *Nat. Mater.* **9**, 205–213 (2010).
12. Oh, J., Yuan, H.-C. & Branz, H. M. An 18.2%-efficient black-silicon solar cell achieved through control of carrier recombination in nanostructures. *Nat. Nanotechnol.* **7**, 743–748 (2012).
13. Ko, E. *et al*. Electrochemical Fabrication of Nanostructures on Porous Silicon for Biochemical Sensing Platforms. *Anal. Sci.* **32**, 681–686 (2016).
14. Vepachedu, V., McAtee, P. D. & Lakhtakia, A. Nonexhibition of Bragg phenomenon by chevronic sculptured thin films: experiment and theory. *J. Nanophotonics* **11**, 036018–1-15 (2017).
15. Mackay, T. G. On the effective permittivity of silver-insulator nanocomposites. *J. Nanophotonics* **1**, 019501–1-5 (2007).
16. McLachlan, D. S., Priou, A., Chenerie, I., Issac, E. & Henry, F. Modeling the Permittivity of Composite Materials with a General Effective Medium Equation. *J. Electromag. Waves Appl.* **6**, 1099–1131 (1992).
17. Mackay, T. G. & Lakhtakia, A. Percolation thresholds in the homogenization of spheroidal particles oriented in two directions. *Opt. Commun.* **259**, 727–737 (2006).
18. Martín-Palma, R. J. & Martínez-Duart, J. M. Accurate determination of the optical constants of sputter-deposited Ag and SnO_2 for low emissivity coatings. *J. Vac. Sci. Technol. A* **16**, 409–412 (1998).
19. Martín-Palma, R. J., Vázquez, L., Martínez-Duart, J. M. & Malats-Riera, A. Silver-based low-emissivity coatings for architectural windows: Optical and structural properties. *Sol. Energy Mater Sol. Cells* **53**, 55–66 (1998).
20. Martín-Palma, R. J., Gago, R., Vinnichenko, M. & Martínez-Duart, J. M. In-depth optical and structural study of silver-based low-emissivity multilayer coatings for energy-saving applications. *J. Phys. D: Appl. Phys.* **37**, 1554–1557 (2004).
21. Kim, S. Y. & Vedam, K. Analytic solution of the pseudo-Brewster angle. *J. Opt. Soc. Am. A* **3**, 1772–1773 (1986).

Acknowledgements

R.J.M.-P. thanks *Ministerio de Educación, Cultura y Deporte* (Spain) for funding under grant reference number PRX17/00095. P.D.M. and A.L. thank the Charles Godfrey Binder Endowment at Penn State for continued support of their research activities. R.R. thanks the Egyptian Ministry of Higher Education, Missions section, for funding under Joint Supervision grant, call 2015–2016.

Author Contributions

R.J.M-P. and A.L. conceived and supervised the study and designed the experiments. P.D.M. carried out the specular reflectance measurements. R.R. fabricated the n-PS and hybrid n-PS/Ag layers, acquired the FESEM images, and was in charge of the overall reflectance optical characterization. R.J.M-P. drafted the initial version of the manuscript. All the authors commented on the results, provided ideas for the study, and reviewed the manuscript.

Additional Information

Competing Interests: The authors declare no competing interests.

Publisher's note: Springer Nature remains neutral with regard to jurisdictional claims in published maps and institutional affiliations.